14.4 HOW WILL X-BAND ATTENUATION AFFECT TORNADO DETECTION IN THE CASA IP1 RADAR NETWORK?

Keith A. Brewster[1], Erin C. Fay[1,2] and Francesc Junyent[3]
[1]Center for Analysis and Prediction of Storms, University of Oklahoma
[2]School of Meteorology, University of Oklahoma
[3]Dept. of Electrical and Computer Engineering, University of Massachusetts

1. INTRODUCTION[.]

The Engineering Research Center for Collaborative Adaptive Sensing of the Atmosphere (CASA) was recently established as in order to build and test a network of low-power, low-cost radars that could utilize Distributed Collaborative Adaptive Sensing (DCAS) to provide detailed information in the lowest levels of the atmosphere (McLaughlin et al., 2005). The lowest 1-to-3 km of the troposphere is not well sampled by the current United States WSR-88D (NEXRAD) operational radar network due to the radar spacing and the earth's curvature. In order to utilize a radar antenna just over 1 m in diameter and to eventually utilize low-cost solid-state transmitters and electronic beam steering, radars in the X-band (3-cm wavelength) were chosen for the network. Due to the power and size limitations, the radars will have a nominal range of 30-km (for 10 dBZ weather targets).

1.1. CASA IP1-A Network

The first test bed, IP1, for the DCAS radar concept will test the ability of the radars to sense and pinpoint low-level wind hazards from severe convective storms (Brotzge et al. 2005). The locations of the radars in the initial IP1 network (IP1-A) were planned to achieve coverage below the WSR-88D NEXRAD radar network 0.5 elevation beam, to provide a large area of overlap of the radars, include a significant fraction with intersecting angles that can provide dual-Doppler wind coverage (Brewster et al. 2005). The area is also upstream of a major metropolitan area, in a region with relatively high tornado occurrence. A map of the IP1-A radar network is shown in Fig 1.

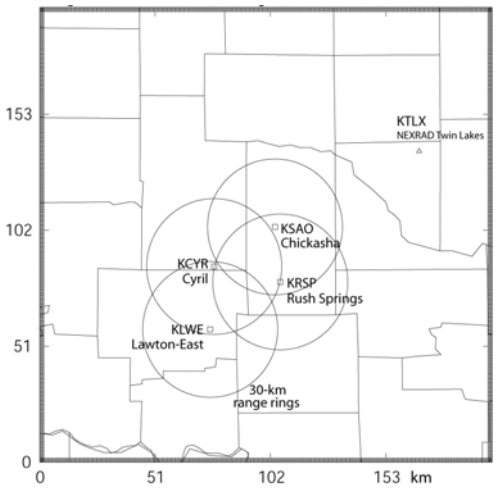

Fig. 1. CASA IP1-A Network in South-western Oklahoma. The CASA radars are at the center of the 30 km range rings. The location of the Oklahoma City WSR-88D (KTLX) radar is also shown.

1.2. Attenuation and Detection

A disadvantage of using X-band radars for weather detection is the amount of signal attenuation that can be experienced in rain. The attenuation is particularly severe in moderate-to-heavy rain, where the reflectivity factor is greater than 40 dBZ.

As long as a detectable signal can be obtained by the radar after attenuation, velocity measurements can be made and estimates of the attenuation rate can be applied to correct the reflectivity values. Dual-polarametric measurements can be particularly effective for correction of attenuation (e.g., Lim and Chandrasekar 2005). However, once the attenuated signal falls below the sensitivity of the radar, velocity measurements cannot be obtained and there is the possibility of becoming blind

[.1]Corresponding author address: Keith A. Brewster, CAPS/Univ. of Oklahoma, Norman, OK 73019 kbrewster@ou.edu

to weather hazards if the feature cannot be viewed by at least one of the network radars. The goal of this study is to quantify the extent that attenuation will prevent detection of tornadoes in the IP1-A network. This will allow demonstration of the advantages of the overlapping collaborative coverage, set reasonable expectations for network performance before deployment, and will aid in the design of any future network expansion.

2. METHOD

In order to estimate the impact of X-band attenuation on the individual radars and on the radar network, we use S-band (10-cm) WSR-88D radar data that are largely unaffected by rainfall attenuation, and remap the S-band data to a high resolution Cartesian grid. Those gridded data are re-sampled to emulate the radar data that would be collected by each CASA radar. The emulation includes an estimate of the attenuation. The attenuated signal strength at the tornado location is compared to the estimated sensitivity of the radar at that range and a detection (or miss) is determined based on whether the attenuated signal is stronger (or weaker) than the radar sensitivity at that point. Each step of the process is detailed in this section.

2.1. Remapping S-band Radar Data

Archived Level-II WSR-88D data are obtained for each case from the archives of the National Climatic Data Center and are remapped to a Cartesian grid with 1-km horizontal spacing and a stretched vertical coordinate with an average vertical spacing of 400 m. The minimum vertical grid spacing is 40 meters near the ground with the first level at 20 meters above the ground. The remapping is done using software from the ARPS Data Analysis System (ADAS). The remapper fits the data near each grid point to a local function in a least-squares sense. The function is quadratic in the horizontal and linear in the vertical dimension. This has the effect of applying a grid-scale filter to high-resolution data and a second order interpolation where the grid array is more dense than the data. The original reflectivity data have a resolution of 1 km in range and 1 degree in azimuth. Vertical resolution is dependent on the volume coverage pattern used, but is generally about 1-2 degrees in elevation angle for the low angles important for this study.

Reflectivity filling is used below the height of the WSR-88D radar beam where the reflectivity is considered constant below the beam if the reflectivity at the 0.5 elevation angle is greater than or equal to 25 dBZ.

Once the data have been interpolated to the regular grid, horizontal translation of the grid origin is done to place the observed tornado in various positions in and near the CASA IP1-A network. No terrain variation is used in the Cartesian grid so a uniform vertical translation is used to accommodate any difference between the original radar height and the mean terrain height of the IP1-A area.

2.2. CASA Radar Emulation

Measurements from the CASA radar are emulated by interpolating the Cartesian data to specified points within the radar beam pattern and applying a Gaussian beam weighting function to the interpolated data. 343 points are used in a 7x7x7 template of points, equally spaced in elevation and azimuth relative to the beam width and in range equally spaced over the pulse width.

.

The beam intensity weighting of the interpolated data, R_i, is determined by the following function,

$$R = \frac{\sum R_i \left|W(r)\right|^2 f^4(\theta,\phi)}{\sum \left|W(r)\right|^2 f^4(\theta,\phi)}$$

with the azimuthal and elevation weighting function specified by

$$f^4(\theta,\phi) = \exp\left\{-4\ln 4\left[\left(\frac{\theta_j-\theta_0}{\theta_{ef}}\right)^2 + \left(\frac{\phi_k-\phi_0}{\theta_1}\right)^2\right]\right\}$$

where θ_1 is the antenna beam width (2° for the CASA radars), θ_{ef} is the effective azimuthal beam width determined by the antenna beam width and the rotation rate following the method of Wood and Brown (1989). For the CASA radars rotating at 18°

per second, the effective beam width is found to be 2.16°.

The range weighting function, $|W(r)|^2$, is modeled by a Gaussian function using the radar receiver characteristics assuming a matched receiver and a Gaussian waveform, from Doviak and Zrnić (1993):

$$W(r) = \exp\left[\frac{-(r_i - r_0)^2}{4\sigma_r^2}\right]$$

where r_0 is the range to the center of the gate and

$$\sigma_r = 0.35 c\tau/2$$

where c is the speed of light and τ is the pulse length.

The height of the beam in the grid and the along-surface range is estimated by the four-thirds earth function (e.g. Doviak and Zrnić 1993).

2.3. X-band Attenuation

Two-way attenuation of X-band signals by rainfall is modeled from reflectivity assuming a Laws and Parsons dropsize distribution by the following function

$$K_r = 0.02\left[\frac{Z}{400}\right]^{\frac{1.21}{1.4}}$$

Where K_r is the attenuation (dB/km), and Z is the reflectivity factor (mm^6/mm^3). The attenuation as a function of reflectivity (dBZ) is shown in Fig 2. Significant attenuation is noted for reflectivities greater than 40 dBZ, severe attenuation is noted above 55 dBZ.

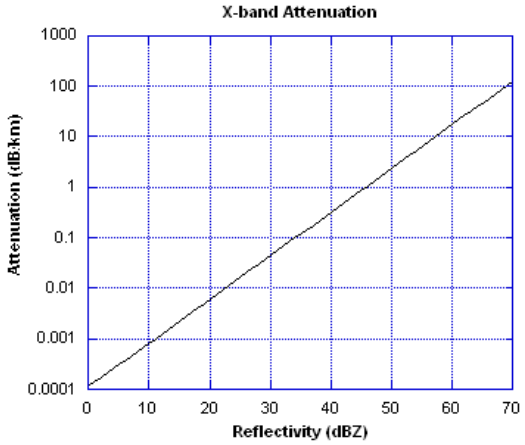

Fig 2. X-band (3-cm) radar attenuation (dB/km) as a function of reflectivity (dBZ).

2.4. CASA Radar Sensitivity

The X-band radar sensitivity expressed as a minimum detectable reflectivity factor (0 dB SNR) as a function of range is modeled by the following function

$$Z_{\min} = 10\log_{10}\left[\left(\frac{R^2 N_i}{\pi^5 |K_w|^2}\right)\left(\frac{8\ln 2}{\pi\theta^2}\right)\left(\frac{2}{c\tau}\right)\left(\frac{\lambda^2 (4\pi)^3 l_m}{P_t G^2}\right)\right]$$

where the variables have meanings and values as shown in Table 1. The radar sensitivity as a function of range is shown in Fig. 3.

Table 1. Variables for Sensitivity Calculation CASA IP1-A Radar

Variable	Name	Value
R	Range	0 – 30 km
N_i	Receiver Noise Power	3.327×10^{-11} mW
$\|K_w\|$	Refractive Index of Water	0.91
θ	3 dB beamwidth	2°
c	Speed of Light	3×10^8 ms^{-1}
τ	Pulse Length	0.6 μs
λ	Wavelength	3.0 cm
l_m	Receiver mismatch loss	1 dB
Pt	Peak Power	12.5 kW
G	Antenna Gain	38 dB

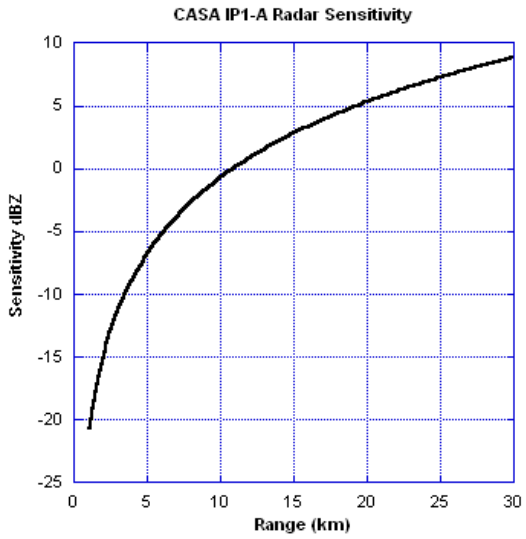

Fig. 3. CASA radar sensitivity expressed as the minimum weather echo detectable as a function of range from the radar.

3. RESULTS

A few storm cases were selected for study, with volume scans every 5-to-6 minutes there are many volume scans available for each case, though there is generally not a large variation from a single volume scan to the next. Some sample times will be shown for each case in this section.

The first case examined was from 8 May 2003. A large violent tornado from a supercell storm caused damage in Moore, Oklahoma on this day. Figure 4 shows the radar reflectivity at 2225. This is near the midpoint of the large tornado of that day. At this time there is a well-defined hook echo and a fairly large area of high reflectivity north of the hook.

Figure 5 is a map of illustrating the ability to detect the tornado in the CASA IP1-A network for data from this volume repositioned in various locations in the region of the network. The green X's represent areas where the attenuated signal in the tornado is expected to be greater than the sensitivity for one or more of the network radars, so velocity measurements can be obtained and presumably the detection algorithms will identify signature from the tornado vortex. The red 0's indicate tested tornado positions where the signal is attenuated to levels

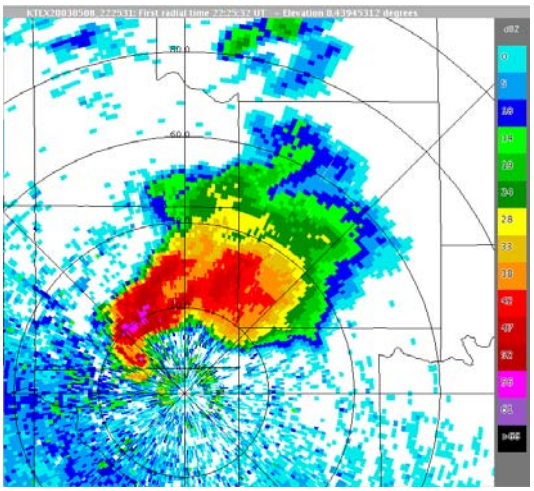

Fig. 4. Oklahoma City (KTLX) radar 0.5 degree scan, 8 May 2003, 2225 UTC. 20-km range rings.

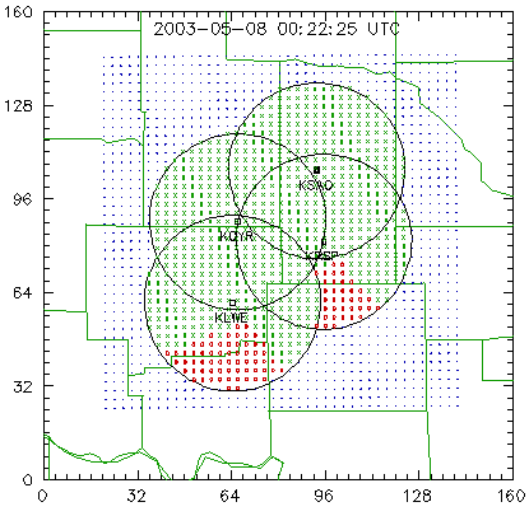

Fig. 5. Regions of potential tornado detections (green X's) and attenuation misses (red 0's) for the tornado of 8 May 2003, 2225 UTC. Blue dots indicate tornado locations tested that were out-of-range of all radars, consistent with the 30 km range rings in black.

Table 2. May 8 Tornado Detection/Miss

Date	Time		Detect	Miss
May 8 03	2225	Single	79%	21%
		Netwk	87	13

below the radar sensitivity for all of the CASA radars within their 30-km nominal range. The areas of red are thus the radar's blind spots for this time.

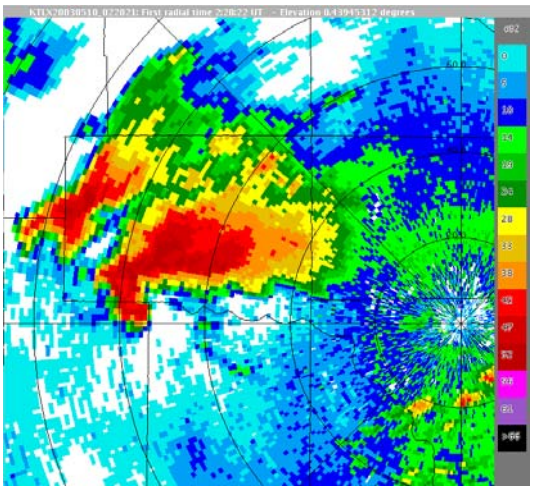

Fig. 6. Oklahoma City (KTLX) radar reflectivity 0.5 degree scan, 10 May 2003, 0220 UTC.

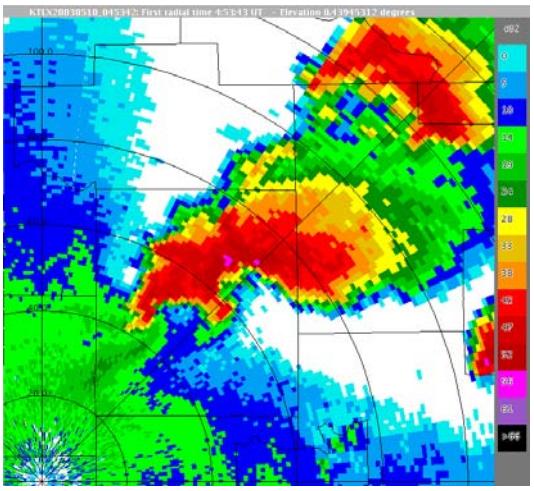

Fig. 8. Oklahoma City (KTLX) radar reflectivity 0.5 degree scan, 10 May 2003, 0453 UTC.

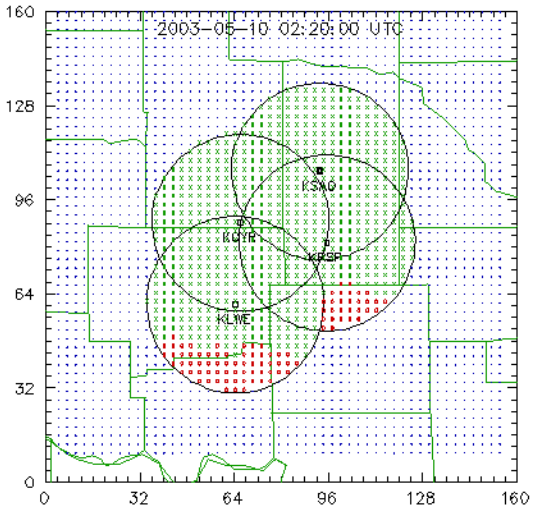

Fig. 7. As in Fig. 5, but for the tornado of 10 May 2003, 0220 UTC

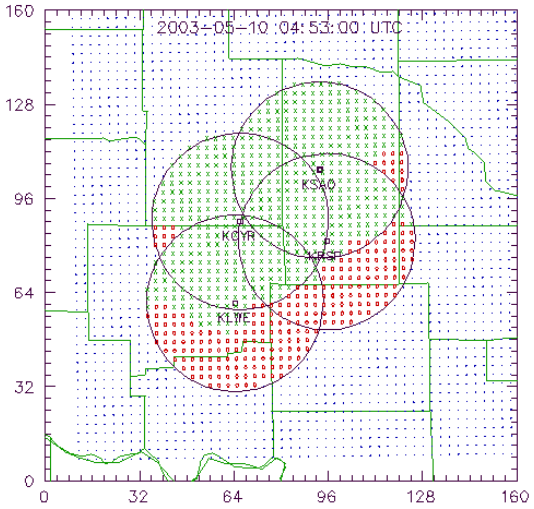

Fig. 9. As in Fig. 5, but for the tornado of 10 May 2003, 0453 UTC

Table 3. May 10 Tornado Detection/Miss

Date	Time		Detect	Miss
May 10 03	0220	Single	81%	19%
		Netwk	88	12
May 10 03	0453	Single	58	42
		Netwk	70	30

Because of the high reflectivity north of the hook echo, if the tornado is located south of a particular radar and at a distance of more than a few kilometers, the radar signal will be attenuated. Thus we see the blind spots south of the southern-most radar sites, Lawton-East (KLWE) and Rush Springs (KRSP). The areas of the corresponding blind spots for the northern two radars can be monitored without attenuation by the southern radars looking north at the tornado through mostly clear air, thus those regions are not blind to the radar network as a whole. This is one of the advantages of the overlapping radar coverage in a collaborative network.

Table 2 is an accounting of the percentage of potential detections among all tornado locations tested within range vs. misses due to attenuation for a radar acting by itself and for the four-radar network as configured for IP1-A for data from this volume scan. The possible detections increase from 79% to 87% by using the collaborative network.

We expect the location of the blind spot to be sensitive to the orientation of the storm echo and the size and strength of the reflectivity in the cell. Another supercell storm passed through Central Oklahoma just a day later, and we show here an analysis of two volume scans from that case.

Figure 6 shows the reflectivity at the beginning of the tornado for the May 9th case (10 May UTC). The supercell storm has a similar shape to the May 8th case, though the orientation of the axis of high reflectivity is rotated to a more E-W orientation relative to the previous case. The blind spots, as depicted in Fig 7, are also similar, but also have a more E-W orientation along the southern edge of coverage area

This storm continued to produce other tornadoes later in its life, and later the area of high reflectivity grew substantially, at one point creating a semi-circle of high reflectivity around the location of a tornado. Fig. 8 is a reflectivity from 0453 UTC, in what might be a worst-case scenario for X-band radar tornado detection. The tornado, as indicated by the radial velocity data (not shown) and the storm reports, was located in the tip of the eastern hook. Fig. 9 confirms the increased size of the blind spot due to the high reflectivity near the tornado on the west, north and northeast.

Table 3 shows the statistics for these two volume scans. The results for the 0220 UTC data are similar to the May 8th case, while the 0453 UTC statistics show the toll of the reflectivity encircling the tornado. An individual radar is blind to the tornado in 42 percent of the locations, but by using the collaborative network the blind area is reduced to 30 percent. Because this pathological configuration of reflectivity occurred late in the lifetime of this supercell storm, the tornado threat from the cell was well documented by this time, so it could be argued that identification of a tornadic threat from this cell was less critical by this time.

We saw a shift in the position of the blind spot due to a slight change in orientation of the supercell in the first two cases examined, so what about a case of a tornado in a storm embedded in northwest flow aloft? Such storms are common in the Midwest in the summertime and can produce tornadoes in the right situation.

On the afternoon of 13 July 2004 a violent tornado (F4) was produced by a supercell storm in Central Illinois under conditions of mid-level northwest flow. The parent thunderstorm had a hook echo and velocity signature on its northwest flank. A low-level reflectivity display of the storm near the initial time of the tornado is shown in Figure 10 for 1936 UTC.

The areas affected by attenuation in this case are shown in Fig 11. Because the storm cell had a smaller reflectivity core the area affected by attenuation is smaller, and the position of the tornado on the northwest flank results in a blind spot to the west of and northwest of each individual radar. Here the collaborative radar network helps to reduce the blind spot as indicated in Table 4, but the relative reduction in the proportional area of the blind spot is not as great as in the supercells moving from the southwest as the overlap in this particular network is more complete in the N-S direction. The smaller size of the blind spot results in a 91.5% potential for detection for

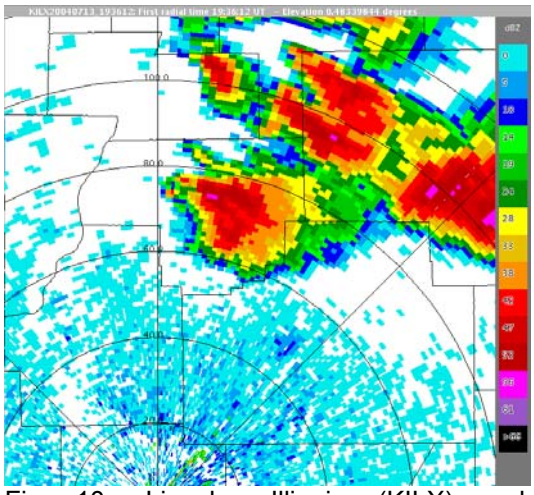

Fig 10. Lincoln, Illinois (KILX) radar reflectivity, 0.5 degree scan, 13 July 2004, 1936 UTC

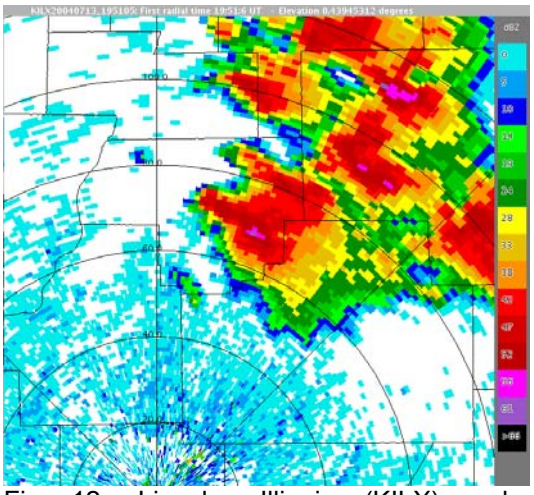

Fig 12. Lincoln, Illinois (KILX) radar reflectivity, 0.5 degree, scan 13 July 2004, 1951 UTC.

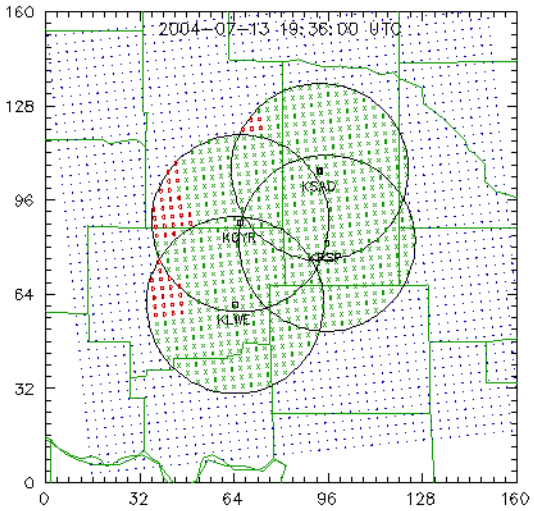

Fig. 11. As in Fig. 5, but for the tornado of 13 Jul 2004, 1936 UTC

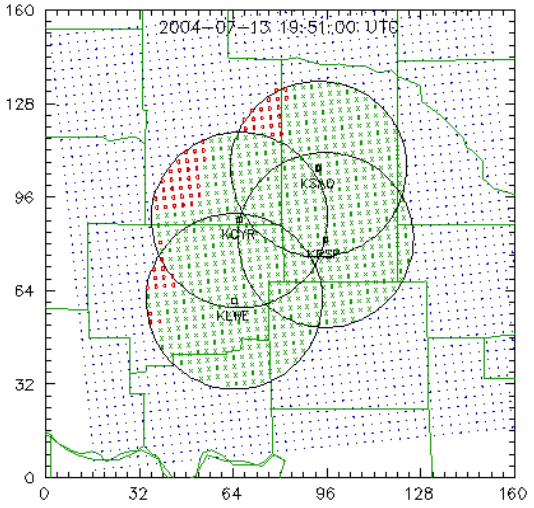

Fig. 13. As in Fig. 5, but for the tornado of 13 Jul 2004, 1951 UTC

Table 4. July 13 Tornado Detections/Misses

Date	Time		Detect	Miss
Jul 13 04	1920	Single	92%	8%
		Netwk	93	7
Jul 13 04	1951	Single	89	11
		Netwk	91	9

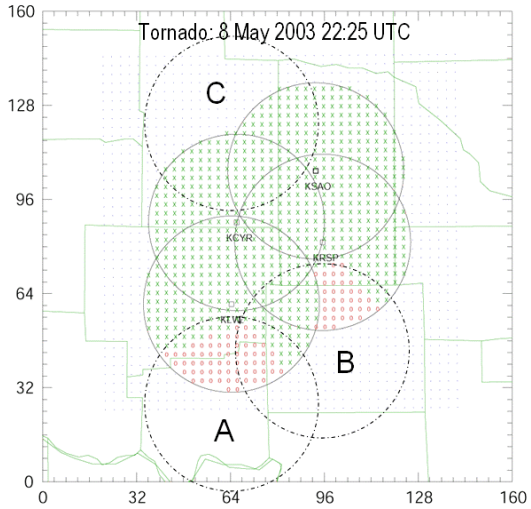

Fig 14. Possible locations of additional radars to cover blind spots noted from 8 May 2004 tornado case. See text for discussion.

an individual radar and 93.3% for the network as a whole.

The results based on the volume scan collected near the end of the tornado's lifetime (15 minutes later, Fig. 12) are little changed, though the area of high reflectivity has increased somewhat resulting in a larger blind-spot for the individual radars (Fig. 13), but the collaborative network would still be able to measure velocities and potentially detect a tornado in 91% of the coverage area.

4. DISCUSSION

4.1. Impact on Network Design

We have seen that the attenuation of X-band electromagnetic waves can produce blind spots in an X-band radar. When configured in a collaborative network the problem is ameliorated as a measurable reduction in the net proportion of the radar coverage area blinded by attenuation is found with a basic four-radar DCAS network. The proportional area that is blind could be reduced further by increasing the size of the radar network and positioning the added radars in a way that would cover the existing blind spot for the most common storm configuration.

For example, consider the results from 8 May, as presented in Fig 14. Two radars, labeled "A" and "B" could be placed just south of the

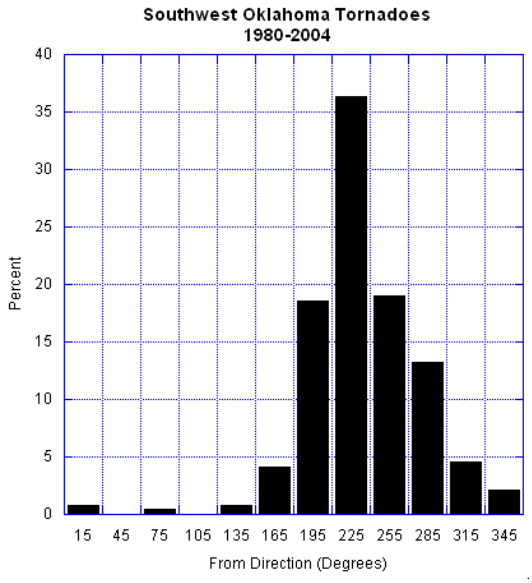

Fig 15. Distribution of tornado motions determined from tornadoes observed from 1980-2004 within 200 km of the center of CASA IP1-A network in Southwest Oklahoma.

IP1-A network, covering the blind spots "anticipated for the Lawton-East and Rush Springs radars. While these radars would have blind spots of their own, the *proportion* of the six-radar network that would be blind would be reduced. Also, the network could be expanded to the north, as depicted by new radar "C". The potential blind spot to the south of radar "C" would be covered by views from the original IP1-A radars, again adding coverage area and reducing the proportional area of attenuation blindness for this case.

The orientation to the blind spots simulated for the case of the 13 July tornado northwest flow storm would argue for expansion of the network to the west of the original net. However, such storms occur much less frequently than storms moving to the east or northeast. To quantify that observation, 25 years of tornado data from the NOAA Storm Prediction Center (SPC) were used to build a quick-look climatology of tornadic storm motion for the area near the IP1-A network.

All tornado reports within 200 km of the center of IP1-A that included a record of beginning and end coordinates were examined to measure the direction of tornado motion. These 276 tornadoes had

damage track lengths greater than 3.2 km (2 miles). The length of the tornadoes may bias the data somewhat, but it also provides some assurance their tracks area representative of the parent storm motion rather than being dominated by some smaller scale movement, such as orbital motion around a mesocyclone. The data were sorted into 30-degree bins and the histogram of storm motions is presented in Figure 15, with bins labeled by the value of the bin center. We can see from the histogram that in Southwest Oklahoma most tornadoes move from the southwest and tornadoes moving from the north or northwest account for less than 10% of the cases in this data set.

4.2. Future Work

In ongoing work we are examining additional volume scans from the storms presented here, and we will be looking at other tornado cases, including more unusual storms than the supercells presented here. Ideally the statistics of anticipated attenuation in the network would be weighted by the local climatology of tornadic storms, including storm motion and a variety of storm morphologies.

5. ACKNOWLEDGMENTS

This work was supported by the Engineering Research Centers Program of the National Science Foundation under NSF Award Number 0313747. The authors have benefited from discussions with engineers in the CASA project including Tian Yu and Robert Palmer. Nathan Snook, Vijay Lakamraju and Eric Lyons provided valuable feedback and testing of the radar emulation software. Subsetting of the tornado data was accomplished using the SeverePlot program provided by John Hart of the SPC.

6. REFERENCES

Brewster, K., L. White, B. Johnson, and J. Brotzge, 2005: Selecting the Sites for CASA NetRad, a Collaborative Radar Network. Preprints, Ninth Symposium on Integrated Observing and Assimilation Systems for the Atmosphere, Oceans, and Land Surface (IOAS-AOLS), AMS Conf., San Diego, CA.

.

Brotzge, J., M. Zink, D. Westbrook, K. Brewster, B. Johnson, B. Philips and M. Preston, 2005: CASA's first test bed: Integrative Project #1. 32nd Conference on Radar Meteorology, Albuquerque, NM, AMS, Boston. This CD.

Doviak, R.J. and D.S. Zrnić, 1993: *Doppler Radar and Weather Observations, Second Edition*. Academic Press, New York, 562 pp.

Lim, S. and V. Chandrasekar,2004: Reflectivity retrieval in a networked radar environment, *Proc. IEEE International Geoscience and Remote Sensing Symposium*, Anchorage, AK, 20-24.

McLaughlin, D.J., V. Chandrasekar , K. Droegemeier., S. Frasier, J. Kurose, F. Junyent1, B. Philips, S. Cruz-Pol, and J. Colom, 2005: Distributed Collaborative Adaptive Sensing (DCAS) for improved detection, understanding and predicting of atmospheric hazards. *Preprints, 9th Symp. On Integrated Obs. and Assimilation Systems for the Atmos., Oceans, and Land Surface*, San Diego, CA, Amer. Meteor. Soc.

Wood, V.T. and R.A. Brown, 1997: Effects of radar sampling on single-Doppler velocity signatures of mesocyclones and tornadoes. *Wea. Forecasting*, **12**, 928-938.